Results in Engineering 18 (2023) 101077

Contents lists available at ScienceDirect

Results in Engineering

journal homepage: www.sciencedirect.com/journal/results-in-engineering

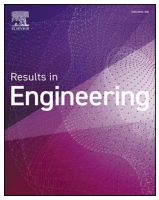

Machine learning algorithms in wood ash-cement-Nano TiO_2-based mortar subjected to elevated temperatures

Akeem Raheem [a,b], Bolanle Ikotun [a], Solomon Oyebisi [c,*], Anthony Ede [c]

[a] Department of Civil Engineering, University of South Africa, Johannesburg, 1710, South Africa
[b] Department of Civil Engineering, Ladoke Akintola University of Technology, Ogbomoso, Nigeria
[c] Department of Civil Engineering, Covenant University, Ota, Nigeria

ARTICLE INFO

Keywords:
Cleaner production
Compressive strength
Elevated temperature
Green-synthesised nano titanium
Machine learning algorithm
Waste valorization

ABSTRACT

Mortar is subjected to high temperatures during fire attacks or when it is near heat-radiating equipment like furnaces and reactors. The physical and microstructure of mortar were considerably altered by high temperatures. In this investigation, the effects of elevated temperatures on the flexural and compressive strengths of wood ash (WA) cement mortar modified with green-synthesised Nano titanium oxide (NT) were examined. In order to produce mortar samples, the cement was replaced with 10% WA, and 1–3% NT by weight of binder were added at constant water-binder ratio. The specimens were heated to 105, 200, 400, 600, and 800 °C with an incremental rate of 10 °C per min in the electric furnace for a sustained period of 2 h to measure their strengths. The machine learning algorithm of artificial neural networks with Levenberg-Marquardt backpropagation training techniques of different network architectures was engaged to predict the compressive strength of WA-cement-NT-based mortar produced. The findings showed that higher temperatures reduced compressive strength after 400 °C and flexural strength after 200 °C. The mortar specimen with a 3% NT addition showed the highest residual compressive strength increase, ranging from 18.75 to 27.38%. Compared to compressive strength, flexural strength is more severely affected by high temperatures. The backpropagation training algorithm revealed that each hidden layer displayed its unique strong prediction. However, Levenberg-Marquardt backpropagation training technique of 7–10-10-1 network structures yielded the best performance metrics for training, validation, and testing compared to 7-10-10-10 and 7-10-1 network architectures.

1. Introduction

Recently, more focus has been placed on how concrete and mortar behave when temperatures are high. When a fire is present or when mortar and concrete are in close proximity to heat-radiating machinery like furnaces and reactors, they are subjected to high temperatures. High temperatures are one of the elements that contribute to the deterioration of mortar and concrete, which affects the resilience of concrete structures [1]. Mortar and concrete both underwent considerable physical and chemical changes at high temperatures. According to Arioz [2], high temperatures have a significant impact on cement paste, aggregate characteristics, and the bond between the cement paste and aggregate in mortar or concrete.

Because mortar and concrete have a poor coefficient of thermal conductivity, heat movement through them is slow. Due to the delayed process, there was a considerable temperature gradient between the exterior surfaces of the mortar or concrete and their interior cores, which caused further damage as the heat increased [3,4]. Hertz [5] noted that calcium silicate hydrate released chemically bound water at 110 °C while microcracks started to appear in the material at 300 °C as a result of dehydration of the matrix and thermal expansion of the aggregates. The characteristics of the material (the type of aggregate and cement used), the moisture level, the size of the fire, and the addition of additives all have a significant impact on how severely mortar or concrete components are damaged by elevated temperatures. The goal of this study is to determine the best way to incorporate additives into mortar to minimize heat transmission.

To enhance the mechanical and durability properties of mortar and concrete, agro-industrial waste products are utilized and the results are promising. For examples, fly ash [6,7], rice husk [8–10], maize cob [11,

* Corresponding author.
E-mail addresses: aaraheem@lautech.edu.ng (A. Raheem), ikotubd@unisa.ac.za (B. Ikotun), solomon.oyebisi@covenantuniversity.edu.ng (S. Oyebisi), anthony.ede@covenantuniversity.edu.ng (A. Ede).

https://doi.org/10.1016/j.rineng.2023.101077
Received 16 January 2023; Received in revised form 4 April 2023; Accepted 5 April 2023
Available online 12 April 2023

12], wood ash [13–15], silica fume [16,17], shea nut shell ash [18], cashew nutshell ash [19], and palm oil fuel ash [20] are the agro-industrial waste materials that have been extensively researched. For instance, Raheem and Adenuga [14] investigated the prospects of wood ash as a partial replacement of cement in the production of concrete. The findings showed that the slump and compacting factor of concrete containing wood ash beyond 10% replacement level becomes more workable as the wood ash content increases, signifying that less water is needed to make the concrete workable. Additionally, after 7–90 days of curing, concrete with 5 and 10% wood ash has greater strength than the control. Yang et al. [15] studied the effects of wood ash on properties of concrete and flowable fill. The addition of wood ash to RCC was found to be beneficial for compaction and lowering the likelihood of segregation. Additionally, the addition of wood ash to mixtures of flowable fill can help improve flow, reduce bleeding and subsidence, and provide controlled strength, particularly when mixed with class C or class F fly ash. The use of wood ash in this study is justified, among other things, by these factors.

In studies on elevated temperature, AbdulAwal and Shehu [21] assessed the performance of high-volume palm oil fuel ash (POFA)--based concrete when exposed to elevated temperature and concluded that concrete containing 50% POFA performed better than typical ordinary Portland cement (OPC) concrete at high temperatures. Additionally, Demiral and Kelestemur [3] considered the impact of increased temperature on the mechanical characteristics of concrete containing silica fume and finely ground pumice (FGP). The study's conclusions demonstrated that concrete with a high amount of FGP had a low compressive strength and low ultrasonic pulse velocity, which helped to mitigate the extreme effects of high temperature on it. Kaya et al. [6] investigated the behavior of class F fly ash based geopolymer mortars subjected to elevated temperatures of 200, 400, 600, and 800 °C. It was observed that there was an increase in the flexural and compressive strengths of some geopolymer mortars after high temperature exposure. In general, geopolymer mortars exhibited better performance at elevated temperatures in comparison to control cement mortar mixture. Donatello et al. [22] investigated the physical and chemical modifications brought about by high volume fly ash cement pastes being heated to temperatures of up to 1000 °C. The study found that, in contrast to OPC paste, fly ash-cement paste had greater residual strength. Aydin and Baradan [23] looked into how fly ash and mortar pumice responded to high temperatures. The findings demonstrated that adding fly ash to pumice aggregate mortar improves the mortar's resistance to high temperatures.

In order to improve the performance of mortar and concrete at high temperatures, the incorporation of nanoparticles has also been researched. The effects of extreme heat on the characteristics of cement mortars comprising heavyweight aggregates and nano silica were evaluated by Horszczaruk et al. [24]. According to the study, adding nano silica up to 3% by weight improved cement mortar resilience at high temperatures up to 200 °C, after which the effect is less noticeable. Similarly, Ibrahim et al. [25] examined the fire resistance of a high-volume fly ash mortar containing nano silica. The findings demonstrated that mortar specimens containing fly ash and nano silica had significant residual strengths after being exposed to 700 °C. Despite numerous research on the effects of supplementary cementitious materials and nanomaterials on the mechanical properties of mortars exposed to high temperatures, little or no study has been conducted on performance of wood ash-cement based mortars exposed to elevated temperatures. Because of this, this study was conducted.

As a result of their artificial intelligence mimicking the neurons in the human brain, machine learning algorithms (MLAs) are constantly growing in the scientific and technological discourse. It creates a system out of data sets and discovers patterns and connections between different factors and groups of factors that would be difficult to carry out manually [26]. There are three layers in the machine learning algorithm: input, hidden, and output. Neurons from the hidden layer are mixed with input components in the input layer. However, the goal factor that the hidden layer received makes up the output layer [26]. As a result, the entire learning process takes place in the hidden layer, where interconnections between neurons are discovered. Machine learning algorithms have been used in numerous research to forecast strength of mortar and concrete mixes subjected to elevated temperatures [27–29]. Asteris et al. [27] predicted the cement-based mortars compressive strength using machine learning techniques such as support vector machine, random forest, decision tree, AdaBoost and k-nearest neighbours. The results showed that the highest prediction accuracy was obtained from the AdaBoost (Adaptive Boosting) and random forest models. Bingol et al. [28] investigated the neural networks analysis of compressive strength of lightweight concrete after high temperatures (up to 700 °C). The compressive strength of lightweight and semi-lightweight concretes with pumice aggregate exposed to high temperatures was modelled using an artificial neural network (ANN) technique. The target temperature, the ratio of pumice to aggregate, and the length of the heating process were the model's inputs, and its output was the concrete's compressive strength. The ANN's projected values were in accordance with the experimental data, and the outcomes showed that the model could accurately estimate compressive strength. Moreover, Najm et al. [29] studied the mechanical properties, crack width, and propagation of waste ceramic concrete subjected to elevated temperatures (100, 200, and 300 °C). The application of machine learning models such as artificial neural networks (ANN) and multiple linear regression (MLR) was employed to predict the compressive and tensile strength of concrete. The linear coefficient correlation (R^2) and mean square error (MSE) were evaluated to investigate the performance of the models. Based on the computational analysis, it was found that the developed MLR model shows higher efficiency than ANN in predicting the compressive and tensile strength of Portland cement concrete, waste ceramic concrete, and waste ceramic-fibre concrete. However, the rapidly evolving technology is predicted to advance social modernisation to completely new heights. One such amazing development is neural networks. Simulated neural networks (SNNs), also known as artificial neural networks (ANNs), are a machine learning application that simulates human-like artificial intelligence (AI) systems. As a result, the ANN of machine learning algorithm was used in this study because of its adaptability, effectiveness, fault toleration, multitasking, capacity to function with incomplete knowledge, and the capacity to understand intricate links between input and output patterns that would be challenging to model using traditional techniques [30,31].

This study examined the impact of high temperatures on the compressive and flexural strength parameters of WA-cement-based mortars modified with nano titanium (NT). In order to produce mortar samples, the cement was replaced with 10% of WA, and 1, 2, and 3% NT by weight of binder were added while keeping a constant water-binder ratio (w/b) throughout all mixes. The specimens were subjected to tests to ascertain their residual compressive and flexural strengths after being heated in an electric furnace to temperatures of 200, 400, 600, and 800 °C. The artificial neural networks were engaged to train the mix design datasets using and the Levenberg-Marquardt, Bayesian Regularization, Scaled Conjugate Gradient backpropagation training algorithms. By evaluating the metrics for measuring the efficacy of each technique, the most effective algorithm for forecasting compressive strength of WA-cement-NT-based mortar was discovered. Therefore, these results aid in understanding how well wood ash-cement-based mortar performs at high temperatures. Additionally, it offers the reference data for developing a framework for high temperature-resistance products utilizing cement and nanomaterials.

2. Materials and method

2.1. Materials

The Cement (CEM 1, 52.5 N), wood ash (WA), and water used were

sourced from South Africa. Tables 1 and 2 present the properties of cement and WA used. According to Table 2, which lists the oxide compositions of the WA, the pozzolan is appropriate for usage because it has a $SiO_2 + Al_2O_3 + Fe_2O_3$ content of 77.67% which is greater than 70%. Instead of the exorbitantly expensive European Silica Standard Sand (ESSS), South Africa Silica Sand (SASS) was utilized, consisting of diameters 0.8–1.8 mm, 0.4–0.85 mm, and 600 mm in that sequence. Fig. 1 shows the SASS and ESSS grading analysis [32]. Fig. 1 shows that both SASS and ESSS compared favourably, with fineness modulus (FM) of 3.5 and 3.45, respectively. The green-synthesised Nano-TiO_2 (NT) was processed and obtained from Nigeria.

2.2. Synthesis of Nano-TiO_2

The green-synthesised Nano-TiO_2 (NT) was biogenically produced utilizing a Cola nitida pod extract. To make the extract, 1.5 g of the milled pod was combined with 150 ml of distilled water and heat for an hour in a water bath at 60 °C. The extract was centrifuged at 4000 rpm for 20 min after filtering through Whatman No. 1 filter paper. After that, the extract was added to 600 ml of TiO_2 solution by mixing 0.5 g of TiO_2 with 0.6 ml of water, producing the NT. The mixture was prepared at 30 ± 2 °C room temperature and left for approximately 2 h [32,35]. An alteration in the solution's colour that was seen visually until it stabilized, as illustrated in Fig. 2, was used to detect the formation of Nano-TiO_2 (NT). Fig. 3 displays the morphologies of NT. NT particles are spherical in shape, as shown in Fig. 3a by the scanning electron microscope (SEM), and they are approximately 38 nm in size, as shown in Fig. 3b by the transmission electron microscope (TEM).

2.3. Preparation of mortar specimens

There were five different types of mortar specimens made, with the codes A, B, C, D, and E. CEM1 and SASS, which are exclusively used as the control experiment, are included in Category A. A 90% of CEM1, 10% WA, and SASS are found in Category B. A 90% CEM1, 10% WA, SASS, and 1, 2, and 3% NT, respectively, are present in Categories C, D, and E. The mortar pastes were molded into 50 mm cubes for compressive and 40 × 40 × 160 mm prisms for flexural strengths tests in accordance with SANS 196–1:2006 [34] guidelines. The blended cement mixes were prepared by mixing CEM1 and WA in the dry state for successive periods of 5 min until homogeneity was achieved. The mortar was prepared with a blended cement to sand ratio of 1:3 and a water/binder (w/b) of 0.5. It had been established that 10% WA substitution with up to 3% NT at w/b of 0.5 exhibited the best results for workability and strength properties, and for structural purposes [14,36]; hence, this was employed in this study. Since NT is a liquid, it was used as a percentage replacement for water during mixing to avoid increasing the mix's w/b, as recommended by Berra et al. [37] and Horszczaruk et al. [24]. The mortar's ingredient mixing ratio is shown in Table 3.

Initially, the mortar samples were stored in humid air for 24 h at 20 °C and 90% relative humidity. After that, the samples were removed from the moulds and cured for 56 days at 25 ± 3 °C.

Table 1
Properties of cement used [33].

Chemical Composition	Cement	SANS 50197–1 [34]
Insoluble residue, %	2.0	≤5.0
SO_3%	2.0	≤4.0
LOI, %	2,5	≤5.0
Cl^- %	<0.01	≤0.1
Physical Properties		
Setting times:	125	≥45
Initial: minutes	2.5	No requirement
Final: hours		
Specific Area (Blaine): m^2/kg	400	No requirement
Compressive strength		≥20,0
		≥52.5
(Mortar prism EN 196–1):		
At 2 days (MPa)	28	
At 28 days (MPa)	±58	
Soundness:	1	≤10
Le Chatelier Expansion (mm)		
Densities:		
Relative density ± 3.14		
Bulk density, aerated, kg/m^3 1100–1300		
Bulk density, as packed, kg/m^3 ± 1500		
Approximate Volume: 50 kg bag, ℓ ± 33		

Table 2
Oxide compositions of WA used.

Oxide composition	Composition (%)
SiO_2	65.10
Al_2O_3	5.32
Fe_2O_3	7.25
CaO	10.56
MgO	2.75
SO_3	1.62
Na_2O	1.04
K_2O	3.36
$CaCO_3$	4.37
LOI	5.18
LSF	1.23
SR	4.43
AR	6.96

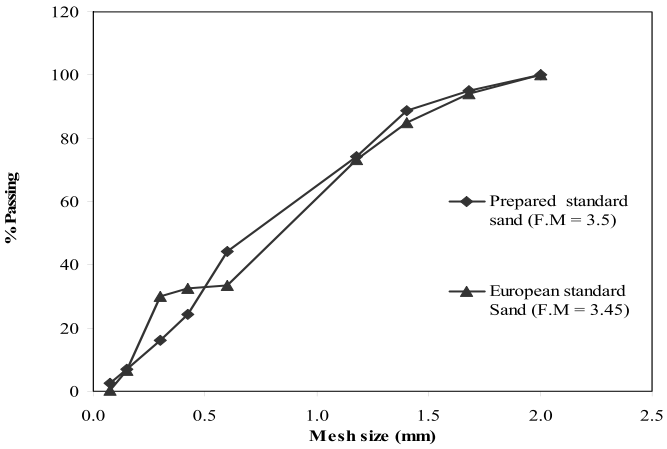

Fig. 1. Grading curves of SASS and ESSS [32].

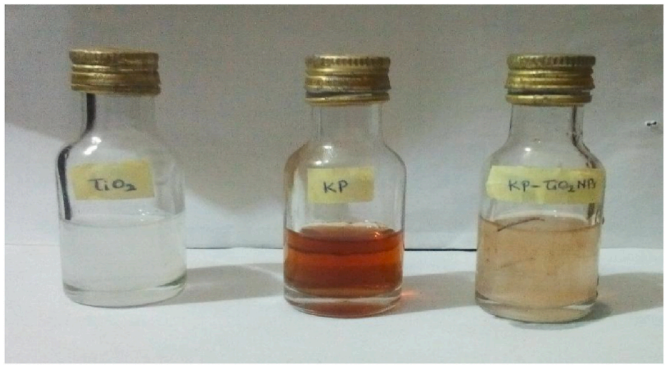

Fig. 2. Preparation of Nano-TiO_2 (NT).

2.4. Heating and cooling regimes

On the 56th day of curing, the samples were removed from the curing tank, cleaned, and weighed before being put into an electric oven to dry

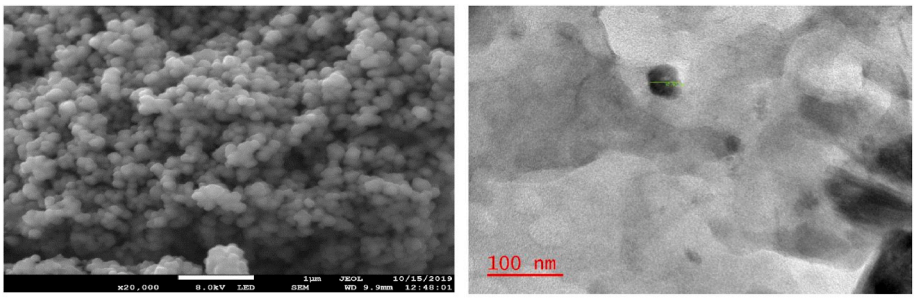

(a) SEM image (b) TEM image

Fig. 3. Morphology of green-synthesised Nano-TiO_2 (NT) [32]. (For interpretation of the references to colour in this figure legend, the reader is referred to the Web version of this article.)

Table 3
Mix proportions of mortar samples.

Sample code	Sample designation	Materials weight (g)				
		CEM 1	WA	SASS	NT	Water
A	100% CEM 1+ SASS (Control)	450	–	1350	–	225
B	90% CEM1 + 10% WA + SASS	405	45	1350	–	225
C	90% CEM1 + 10% WA + 1% NT + SASS	405	45	1350	4.5	220.5
D	90% CEM1 + 10% WA + 2% NT + SASS	405	45	1350	9.0	216
E	90% CEM1 + 10% WA + 3% NT + SASS	405	45	1350	13.5	211.5

for 24 h at a constant temperature of 105 ± 5 °C. A furnace with a capacity of 1400 °C was used for elevated temperature studies. Specimens were subjected to elevated temperatures of 105, 200, 400, 600, and 800 °C with an incremental rate of 10 °C per min in the furnace for a sustained period of 2 h and then air annealed to achieve the thermal steady state. After being gradually heated to the desired peak temperature, the specimens were kept in the furnace for an extra hour to stabilize the temperature on their surfaces. After 2 h of cooling at room temperature, the samples were removed from the furnace and examined. This is comparable to the approach taken by Ref. [24]. Calculations were made to determine the specimens' percentage weight loss as a result of the high temperatures. The percentage weight loss was calculated using the average mass loss of three specimens at each temperature, as given in Eq. (1):

$$\text{Weight loss } (\%) = \frac{\text{Mass at } 20\ ^\circ C - \text{Mass at desired temperature}}{\text{Mass at } 20\ ^\circ C} \times 100\% \quad (1)$$

2.5. Testing of mortar specimens

All specimens' weights were measured prior to testing. The strength measurement was carried out by using UTM by applying compressive force at an incremental rate of 3 kN/s for each test at a particular temperature. A mortar press, ToniPRAX, Model 2010, SN 834, was used to exert stress on the prism specimen until it splits into two equal halves, and the flexural strength was also measured. According to the guidelines in SANS 196–1 [38], compressive and flexural strengths were evaluated using an average of three mortar prisms and cubes, respectively.

2.6. Artificial neural networks

Using input and output training data, neural networks offer the fundamental knowledge needed to identify the ideal operating point. When the neural network is given an input and an output with a corresponding intended or target response, the training is known as supervised training [39–41]. A crucial decision in choosing the overall neural network architecture is the number of neurons in the hidden layers [42]. Even when they do not immediately interact with the environment, these layers have a substantial impact on the outcome. Hence, the number of hidden layers and the number of neurons in each of these hidden levels should be carefully analysed to avoid underfitting and overfitting [42,43].

In order to provide consistent data, adequately address the problems associated with multi-dimensional mapping, and have enough neurons in its hidden layer, this work used backpropagation training techniques with sigmoid hidden neurons and linear output neurons [41]. The network was trained using Levenberg-Marquardt backpropagation algorithm, which ultimately produced appropriate training method results. This benefit is substantial when working with large networks that contain many neurons and can significantly shorten training and evaluation periods [44–48]. In addition, among all available training algorithms in the prediction of mechanical properties, crack width, and propagation of waste ceramic concrete subjected to elevated temperatures, the Levenberg–Marquardt algorithm produced the best ANN prediction [29]. These justify the rationale behind the selection of Levenberg-Marquardt backpropagation algorithm used in this study. However, the function of Levenberg-Marquardt backpropagation is restricted by its computation, which uses the Jacobian, presuming that performance is a mean or sum of squared errors [42]. Therefore, networks trained with these functions must either use the mean squared error (MSE) or sum squared error (SSE) performance function.

As the number of hidden layers rises, the number of model coefficients does as well. To provide reliable and trustworthy estimations of these model coefficients, a large amount of data is needed. These led to the claim that an ANN with two hidden layers was sufficient to accurately represent the majority of functions in the real world [49]. However, ANNs with more than two hidden layers have greater capacity for data learning and testing, which raises prediction accuracy [50]. As a result, this study applied the network architecture called ANN 7-*n*-1, where the first character is the number of input nodes, n is the number of hidden layers ranging from 1 to 3, and third character is the number of output. To analyze how each network architecture's prediction accuracy improved for the compressive strength of mortar [51,50], the number of neurons in each hidden layer was tested from 2 to 14.

In an ANN, training and test sets of data are created from the original data set. The dataset is examined to determine the model's accuracy once a model has been fitted using a subset of the original dataset. Thus, quality training data form the basis of ANN. It is therefore essential to feed the model with high-quality, pertinent, consistent, comprehensive, and uniform data [52]. The neural network was built using a total of seven input variables as training datasets. They are cement, wood ash,

silica sand, Nano titanium oxide, water, curing day, and temperature. A target variable, otherwise called target dataset, is compressive strength. Therefore, compressive strength was predicted based on the training datasets. A 70% of the samples were used for training, 15% for validation, and 15% for testing, in keeping with other pertinent studies on ANNs [53–64]. The mean square errors (MSE) of the training, the validation, and the testing are tracked as several trials are done for the training with changing numbers of neurons in the hidden layer, starting with a low number and progressively increasing it. The hidden layer's neuron count is calculated using the training, validation, and testing sets of data with the lowest mean square errors (MSE) and highest coefficient correlation (R) [53,54,65]. Due to the various starting conditions and sampling, training repeatedly will produce a diversity of results. However, by developing a function and giving the ANN a random stream, this randomness was prevented. The ANN was engaged using MATLAB R2021a version 9.10.0 1602886. Fig. 4 shows the best neural network architecture. The correlation coefficient (R) and mean square error (MSE) were the performance indicators used in this investigation. The forecast's accuracy increases as R-value approaches 1. However, the forecast is more accurate when the MSE is less than 0. The performance metrics are illustrated in Eqns. (2) and (3). The created network model was used to make new predictions based on untrained data. This is important since a model has to be able to forecast new data that has not yet been observed or trained.

$$R = 1 - \frac{\sum_{i=1}^{n}\left(y_i^{pred} - y_i^{true}\right)}{\sum_{i=1}^{n}\left(y_i^{pred} - \overline{y_i^{true}}\right)} \quad (2)$$

$$MSE = \frac{1}{n}\sum_{i=1}^{n}\left(y_i^{pred} - y_i^{true}\right)^2 \quad (3)$$

Tables 4 and 5 present the range and statistical description of data, respectively. Three samples from each of the specimens C, D, and E at 1, 2, and 3% NT, respectively, are included in the data. The dataset has a single target, which is compressive strength (CS). The inputs comprise seven arguments: cement, wood ash (WA), South Africa Silica Sand (SASS), Nano titanium oxide (NT), water, curing day (CD), and temperature (Temp).

Table 4
Range of input and target data.

Constituents	Data type	Unit	Minimum value	Maximum value
Cement	Input	g	405	405
WA	Input	g	45	45
SASS	Input	g	1350	1350
NT	Input	g	4.50	13.50
Water	Input	g	211.50	220.50
Temp	Input	°C	20	800
CD	Input	day	56	56
CS	Output	MPa	16.60	50.21

Table 5
Statistical description of data.

Statistics	NT (g)	Water (g)	Temp (oC)	CS (MPa)
Mean	9	216	346.25	38.39
Median	9	216	200	42.22
Mode	4.5	220.50	20	–
Standard deviation	3.71	3.71	283.49	10.91
Count	48	48	48	48

3. Results and discussion

3.1. Weight loss

Fig. 5 shows the percentage weight loss of mortars due to the impact of high temperatures. As can be seen from Fig. 5, the weight loss increases as the temperature rises. At 105, 200, 400, 600, and 800 °C, specimen A experienced weight losses of 6.5, 7.6, 9.7, 11.8 and 12.2%, respectively. The weight loss increased from 7.6% at 105 °C to 12.6% at 800 °C with WA added to CEM1 in specimen B. The addition of 1% NT to

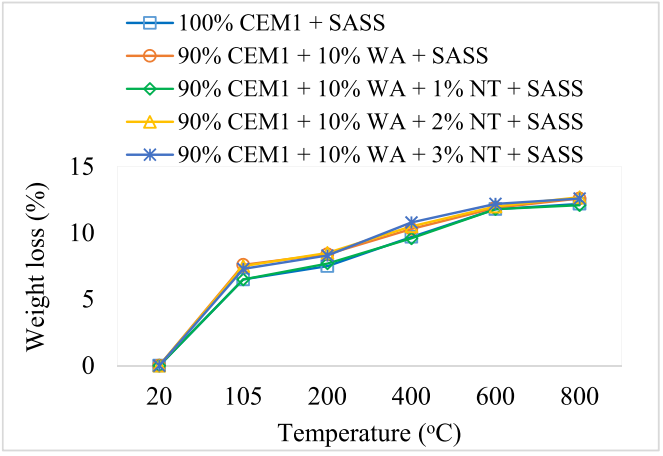

Fig. 5. Percentage weight loss of WA-cement-NT-based mortars at different temperatures.

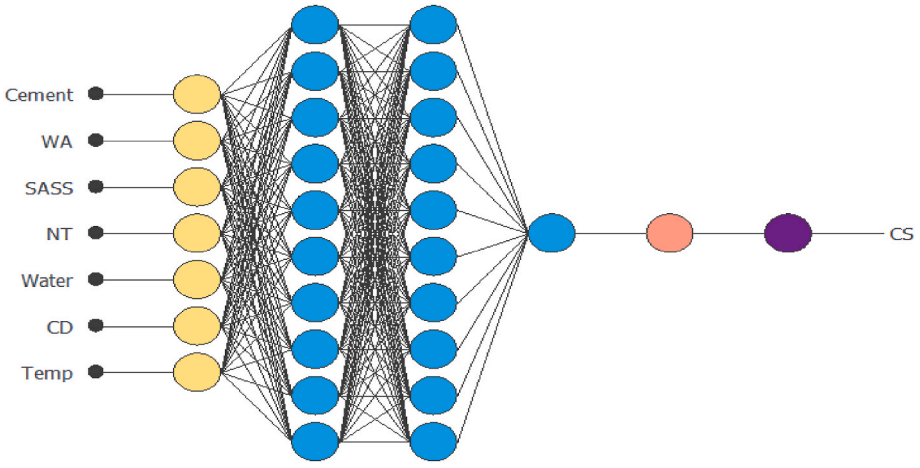

Fig. 4. Best neural network architecture (7-10-10-1).

the binder somewhat lessened the weight loss in specimen C, with the percentage falling from 6.5% at 105 °C to 12.1% at 800 °C. Compared to specimens A, B, and C, specimens D and E have greater percentage of weight loss. The release of bound water in the mortar is thought to be the cause of the weight loss, which increases in percentage as temperatures rise. The evaporable water in the mortar is forced out as the temperature rises, resulting in a loss of mass for the specimens [66,67]. Cement-based composites exhibit considerable mass loss at temperatures above 400 °C [68]. Fares et al. [69] also supported this assertion, where at a high temperature of 400 °C, all the specimens in this investigation experienced a weight loss of roughly 10%. All mortar specimens experienced greater weight losses after the temperature reached 400 °C. With 1% NT added, Specimen C had the smallest percentage improvement in weight reduction.

3.2. Flexural strength

Fig. 6 illustrates the flexural strength of WA cement mortars incorporated with NT when subjected to high temperatures. The flexural strength typically increased up to 200 °C and decreased after that up to an enhanced temperature of 800 °C. At 600 and 800 °C, flexural strength started to drop more quickly. After drying samples at 105 °C for 24 h, the flexural strength rose considerably. As temperature rose from 20 to 105 °C, the strength of specimens A, B, C, D, and E increased from 7.67 to 8.62 MPa, 5.75–8.09 MPa, 6.38–7.57 MPa, 6.25–6.97 MPa, and 5.90–5.93 MPa, respectively. Additionally, at 200 °C, slight increases were seen. These outcomes were comparable to those mentioned by Horszczaruk et al. [24]. There was a decrease in strength after the temperature reached 200 °C. Specimens A, B, C, D, and E recorded 7.11, 6.06, 5,53, 5.91, and 6.01 MPa at 400 °C and 2.31, 2.08, 1.98, 2.25, and 2.16 MPa at 600 °C, respectively, indicating a very considerable strength loss between 400 and 600 °C. At 800 °C, none of the specimens' flexural strengths were greater than 1.00 MPa.

The hardened mortar samples developed micro-cracks because of burning at high temperatures, which reduced their flexural strength. According to Heikal et al. [70], when cementitious composites are exposed to temperatures above 400 °C, micro-cracks begin to form and intensify as the temperature rises, lowering the flexural strength of the material. The majority of cement matrix hydration products completely disintegrate about 800 °C [71]. According to Morsy et al. [72], the development of micro-cracks is what causes the flexural strength to drop as temperature rises from 250 to 800 °C. Additionally, the driving out of free water and a portion of the cement mortar's hydration water due to high temperatures might be responsible for the decrease in flexural strength [72]. Basically, the decrease in flexural strength due to increase in temperature from 400 to 800 °C is due to dehyroxylation of $Ca(OH)_2$.

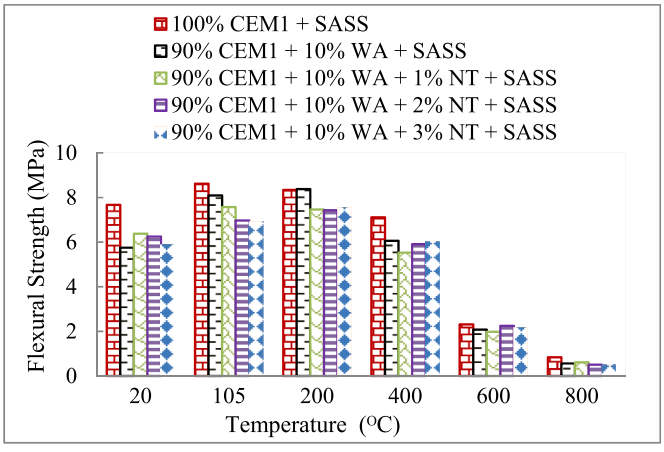

Fig. 6. Flexural strength of WA cement mortars incorporated with NT at elevated temperatures.

The increased micro-cracking is the result of high thermal stresses, which are generated due to the induced temperature gradients up to 800 °C. The addition of NT to WA cement mortar has no appreciable impact on flexural strength at high temperatures.

3.3. Compressive strength

Fig. 7 displays the compressive strength of WA cement mortar specimens modified with NT following exposure to high temperatures. As shown in Fig. 6, the compressive strength of each mortar specimen grew gradually up to the point of 400 °C before abruptly decreasing between that point and 800 °C. These findings are consistent with the pertinent study's results, which showed that the compressive strength of mortar made of nano-metakaolin and cement increased before and after exposure to increasing temperatures of 200–400 °C, but fell above 400 °C [72]. The increase in compressive strength up to 400 °C may be attributed to the additional hydration of unhydrated cement grains because of steam effect under the condition of the so-called internal autoclaving effect [72]. However, the decrease in compressive strength with increase in temperature above 400 °C may be due to the dehydration of calcium hydroxide, generating CaO and H_2O. Strength losses over 400 °C, are mainly caused by calcium carbonate dissociation and subsequent CO_2 escape from $CaCO_3$ [72].

Fig. 8 displays the residual strengths of mortar specimens at various high temperatures. For specimen A (the control), as temperature rose from 20 to 400 °C, the compressive strength increased from 5.54 to 14.63%. As specimen B showed a strength increase of between 13.56 and 23.18% for the same temperature range, higher residual compressive strength was seen with the addition of WA to cement mortar. Only between 7.07 and 12.27% more strength was gained with the addition of 1% NT, as seen for specimen C. The specimen E with a 3% NT addition showed the greatest gains in residual strength, ranging from 18.75 to 27.35%. Ultimately, the replacement of cement with 10% WA and 1–3% NT resulted in better strength at higher temperature (200–400 °C) than the control samples. Due to the dehydration of calcium-silicate-hydrate (C–S– H) and Portlandite ($Ca(OH)_2$) in the binder gel as well as the formation of internal stress, cement deteriorates at high temperatures [73].

The pozzolanic interaction between the cement's $Ca(OH)_2$ and the reactive SiO_2 from the WA, which reduced the amount of $Ca(OH)_2$ in the mixture, may be attributed to specimen B's higher residual compressive

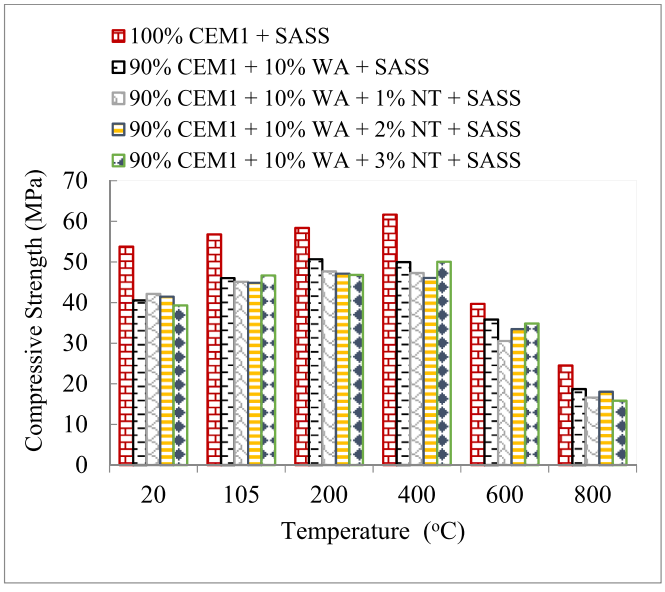

Fig. 7. Compressive strength of WA cement mortars containing NT at elevated temperatures.

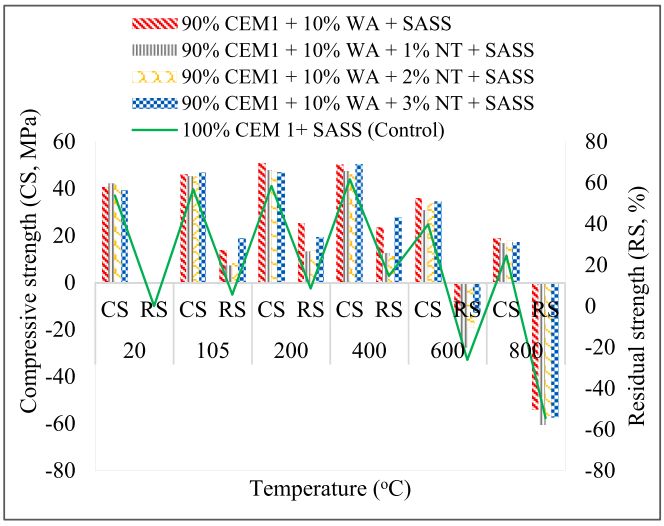

Fig. 8. Residual strength of WA cement mortars containing NT at elevated temperatures.

strength than specimen A's [23]. In a similar vein, the introduction of 3% NT, which improved the microstructure by nano-filling and nucleating, contributed to the increase in compressive strength and is responsible for the maximum residual strength seen in specimen E [70]. Because TiO_2 increases the microstructure of cement paste in this way, natural mortar may benefit from its high temperature resistance because any potential thermal stresses may not be high enough to damage the natural mortar's stronger interfacial transition zone (ITZ).

When exposed to temperatures between 600 and 800 °C, the compressive strength of every specimen significantly dropped; specimens A, B, C, D, and E reportedly decreased by 26.18 and 54.43%, 11.64 and 53.86%, 27.49 and 60.53%, 19.22 and 56.42%, and 12.85 and 57.15%, respectively. Since all specimens lost their strengths at 600 and 800 °C, the elevated temperatures of 600 and 800 °C was particularly problematic. Previous studies have verified the loss of compressive strength of mortar and concrete specimens at elevated temperatures of 400–800 °C [73–75]. The strength decrease of Nano-TiO_2 admixed geopolymer after exposure to temperature above 400 °C, according to Sivasakthi et al. [73], was due to increased geopolymerization and sintering, which improve thermal stability. If not, thermal incompatibility results in destruction. In addition, the coefficient of thermal expansion (CTE) varies with porosity and with the composition of the cement paste [74]. The decrease in compressive strength of Nano-TiO_2-recycled aggregates based-mortars above 400 °C is ascribed to the different thermal properties of cement paste with Nano-TiO_2, inducing additional thermal stresses that cause damage in the weak ITZ of mortars with recycled aggregates [74]. Bastami et al. [75] attributed the decrease in compressive strength to the specimens becoming dehydrated due to the loss of physically bonded water, which has an impact on the mechanical properties. According to a study by Lin et al. [76], concrete specimens underwent substantial deterioration at a high temperature of 800 °C because of the dissolution of the C–S–H gel. This holds true for the mortar specimens under investigation as well. Ibrahim et al. [25] 's further claimed that the extreme strength loss over 700 °C is caused by an excessive build-up of vapour pressure, which results in the specimens developing significant cracks.

3.4. Correlation between flexural strength and compressive strength

The relationship between the flexural strength and compressive strength of WA-cement-NT-based mortar subjected to elevated temperatures is presented in Fig. 9. The datasets comprised the results obtained from 90% CEM1 + 10% WA + 1% NT + SASS, 90% CEM1 + 10% WA + 2% NT + SASS, and 90% CEM1 + 10% WA + 3% NT + SASS at temperatures varied from 20 to 800 °C. After the regression analysis, the power trend line yielded the best-fit equation. The regression equation, as shown in Fig. 9, signified that coefficient of determination (R^2) is 92.88% fit to predict the datasets at 95% confidence and predictive intervals for 56 days of curing. This result aligns with the findings of Morsy et al. [72] where the correlation between the flexural and compressive strengths of blended cement mortars containing nano-metakaolin at elevated temperatures (20, 250, 450, 600, and 800 °C) yielded 87.27% R^2 at 28 days of curing. The slight variation may be attributed to the material properties, days of curing, water/binder ratio, and aggregates/binder ratio. Therefore, this equation can be applied in the prediction of blended cement mortars modified with Nano-TiO_2.

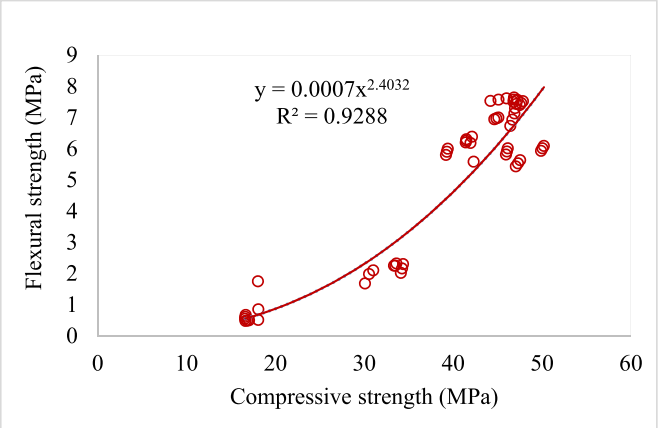

Fig. 9. Relationship between flexural strength and compressive strength.

3.5. Artificial neural networks

3.5.1. Performance metrics

Based on the developed number of network architectures, the Levenberg-Marquardt backpropagation's performance indicators for the compressive strength of WA-cement-NT-based mortar are shown in Table 6–8 for one, two, and three hidden layers, respectively. Comparing the backpropagation training algorithms for 1-hidden layer with 2–14 neurons, as shown in Table 6, 7-4-1 network structures yielded the best metrics for predicting the compressive strength of WA-cement-NT-based mortar. This signified that the number of neurons in the 1-hidden layer

Table 6
Performance metrics for 1- hidden layer with 2–14 number of neurons.

Network architecture	Results	Performance metrics MSE	R
7-2-1	Training		0.99691
	Validation	0.800	0.98784
	Testing		0.99629
7-4-1	Training		0.99920
	Validation	0.194	0.99756
	Testing		0.98962
7-6-1	Training		0.99759
	Validation	0.360	0.97158
	Testing		0.98756
7-8-1	Training		0.99682
	Validation	0.297	0.99611
	Testing		0.99760
7-10-1	Training		0.99736
	Validation	0.300	0.99437
	Testing		0.99787
7-12-1	Training		0.99982
	Validation	0.360	0.97524
	Testing		0.99759
7-14-1	Training		0.87050
	Validation	0.0355	0.98476
	Testing		0.93194

Table 7
Performance metrics for 2- hidden layer with 2–14 number of neurons.

Network architecture	Results	Performance metrics MSE	R
7-2-2-1	Training		0.83780
	Validation	30.100	0.72075
	Testing		0.20272
7-4-4-1	Training		0.99986
	Validation	0.0355	0.99970
	Testing		0.99986
7-6-6-1	Training		0.99853
	Validation	0.140	0.99959
	Testing		0.99858
7-8-8-1	Training		0.99601
	Validation	0.241	0.99710
	Testing		0.99964
7-10-10-1	Training		0.99981
	Validation	0.0359	0.99991
	Testing		0.99992
7-12-12-1	Training		0.99967
	Validation	0.0452	0.98224
	Testing		0.99667
7-14-14-1	Training		0.93463
	Validation	0.0355	0.68256
	Testing		0.72223

Table 8
Performance metrics for 3- hidden layer with 2–14 number of neurons.

Network architecture	Results	Performance metrics MSE	R
7-2-2-2-1	Training		0.90158
	Validation	21.100	0.95041
	Testing		0.86854
7-4-4-4-1	Training		0.64998
	Validation	16.900	0.87096
	Testing		0.48020
7-6-6-6-1	Training		0.99982
	Validation	0.0228	0.06630
	Testing		0.97888
7-8-8-8-1	Training		0.99988
	Validation	0.0247	0.99967
	Testing		0.99951
7-10-10-10-1	Training		0.99989
	Validation	0.0232	0.97793
	Testing		0.98897
7-12-12-12-1	Training		0.96174
	Validation	0.0237	0.98260
	Testing		0.98384
7-14-14-14-1	Training		0.99992
	Validation	0.0119	0.99762
	Testing		0.99986

optimized for the Levenberg-Marquardt backpropagation is four. This result suggests that the best model created for the prediction of compressive strength of WA-cement-NT-based mortar does not actually need a higher number of neurons in the 1-hidden layer. This supports a prior study in which the forecast of building cooling load led to shallow architecture rather than deep networks because of the limited amount of dataset [77]. The free-error performance, as revealed by MSE in Table 6, indicated that 7-4-1 network architecture is about 35–76% more efficient than other network structures. The MSE for 7-14-1 network is lower than 7-4-1- network structure, but the correlation coefficients of 7-4-1- network structure for training, validation, and testing are stronger than the 7-14-1 network architecture. Thus, a 7-4-1- network structure is adjudged as best network in the 1-hidden layer. The reasons for this performance might be accounted for by how quickly 7-4-1 network trains moderate-sized feedforward neural networks (up to several hundred weights) [78,79]. Conversely, when the number of hidden layers increased from one to two and three, as indicated in Tables 7 and 8, the number of neurons in the second and third hidden layers optimized for the Levenberg-Marquardt backpropagation are ten (10) and fourteen (14). These connote that the number of the hidden layers increased with increasing number of neurons. From Table 7, a 7-10-10-1 network architecture produced the best performance metrics compared to other network structures in 2-hidden layer with about 21–99% error-free efficiency. In the same vein, a 7-14-14-14-1 network architecture exhibited the best performance indicators compared to other network structures in 3-hidden layer with about 48–99% error-free efficiency.

A good network topology cannot be inferred solely from the numbers of input and output data. The truth is that a good number of hidden layers can accurately shorten training times with high accuracy. There are numerous methods for standardizing the best number of hidden layers needed for neural networks; however, each time, the estimate relies on the type of database [80,81]. Moreover, Panchal et al. [82] inferred that the best number of hidden units depends on the numbers of input and output units, the number of training cases, the amount of noise in the targets, the complexity of the function or classification to be learned, the architecture of the type of hidden unit activation function, and the training algorithm. On this note, comparisons of the overall accuracy of hidden layers used in this study were made. It is evident in Table 7 that 2-hidden layer with ten number of neurons in each layer (7-10-10-1) yielded the best correlation coefficient for training, validation, and testing of input and output arguments. This is followed by 3-hidden layer with fourteen neurons in each layer (7-14-14-14-1) in Table 8, and lastly, 1-hidden layer with four neurons in the layer (7-4-1) in Table 6. These results infer that the prediction of compressive strength of WA-cement-NT-based mortar using the Levenberg-Marquardt backpropagation training technique reached its best learning at 2-hidden layer network with ten neurons in each hidden layer. The reasons can be attributed to the generalization capacity of multiple layers, which learn all the intermediate features between the input data and high-level classification [83]. In addition, the results corroborate previous studies where an ANN with more hidden layers showed a better capacity for data learning and mining and improved the prediction accuracy [80,83]. For instance, Karsoliya [80] found a subpar performance indication when single layer was used in conjunction with the introduction of intricate and large problems. Then, it was established that in order to get satisfactorily results, the amount of hidden layers must be increased until accuracy is attained.

Although, in principle, there is no reason for a deep neural network. A sufficiently wide neural network with just a single hidden layer can approximate any (reasonable) function given enough training data [83]. There are, however, a few difficulties with using wider and shallow networks with single layer. The main issue is that they are very good at memorization, but not so good at generalization, which is not useful for any practical application. This is why Panchal et al. [82] inferred that neural networks gave better performance as soon as number of hidden neurons and hidden layers increase. Ultimately, the model performs better as the correlation coefficient comes closer to 1. As a result, the performance metrics of the 7-10-10-1 network structure given in Table 7 for the prediction of compressive strength of WA-cement-NT-based mortar showed the best performance.

3.5.2. *Mean squared error (MSE) of performance plot*

In Fig. 10, the best performance and error characteristics for the backpropagation training algorithms for the compressive strength of WA-cement-NT-based mortar are displayed. The best validation performance for the Levenberg-Marquardt, the best training performance of 7-4-1, 7-10-10-1, and 7-14-14-14-1 network architectures at epochs 29, 8, and 4, respectively, was evidently 0.51339, 0.036415, and 0.2860, verifying the outcomes shown in Tables 7–9. The results disclosed that 2-hidden layer network structure with 10 number of neurons in each layer (7-10-10-1) was more error-free efficient than 7-4-1 and 7-14-14-14-1 networks. These results support a relevant work in which the logistic and tanh input functions provided mean squared errors of 0.010 and 0.016 for ANN predictions of cement mortar compressive strength employing seven hidden layer neurons [57]. A network system with better training produces results with the least amount of error and can

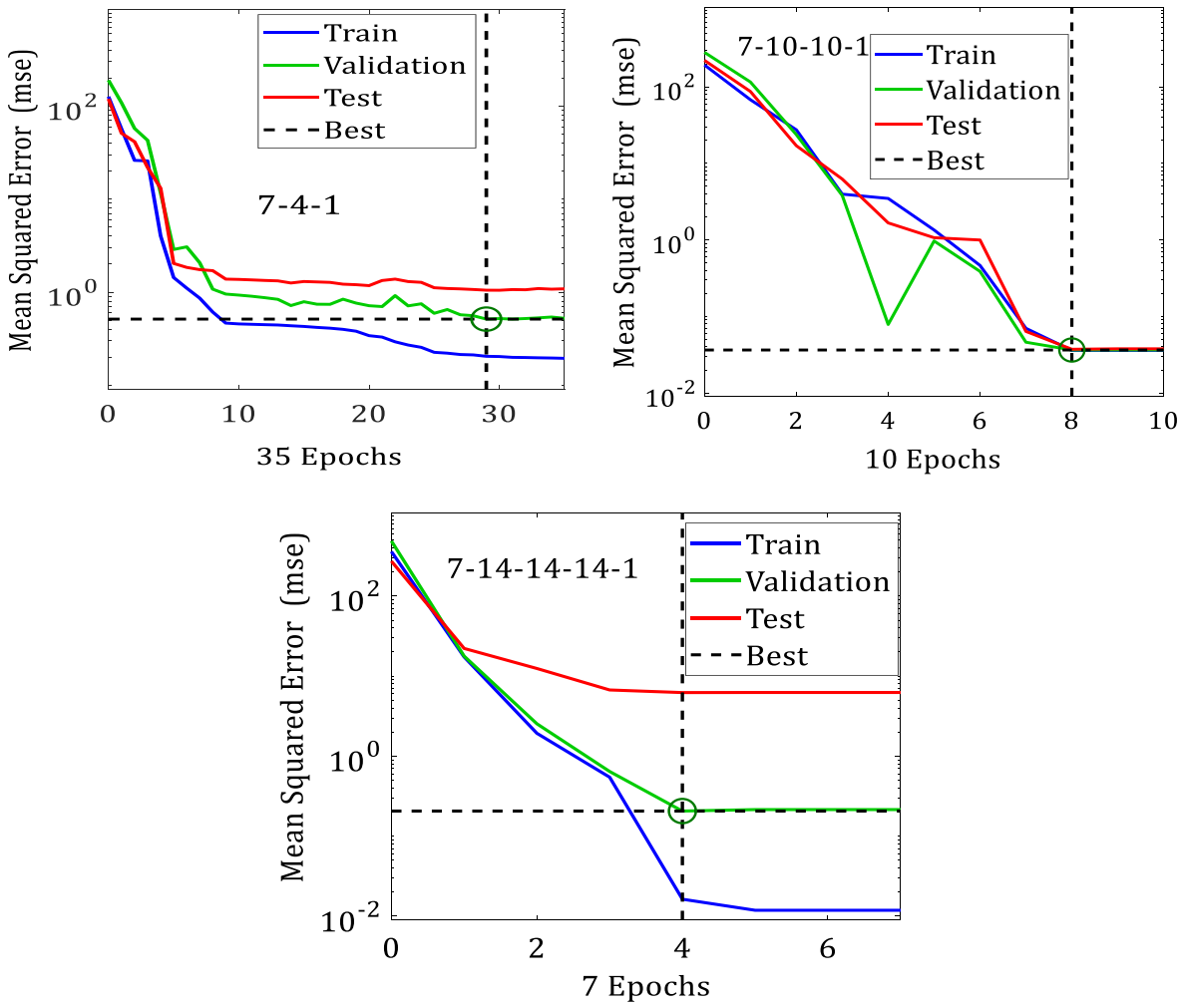

Fig. 10. MSE plots for the best validation performance.

Table 9
Untrained datasets.

S/N	Cement (g)	WA (g)	SASS (g)	NT (g)	Water (g)	CD (day)	Temp (°C)	True value CS (MPa)	Predicted (7-4-1) MPa	Predicted (7-10-10-1) MPa	Predicted (7-14-14-14-1) MPa
1	405	45	1350	4.5	220.5	56	105	46.01	45.64	44.66	44.21
2	405	45	1350	4.5	220.5	56	400	47.06	47.59	47.54	47.42
3	405	45	1350	9	216	56	200	46.97	46.54	47.12	47.21
4	405	45	1350	9	216	56	600	33.49	33.76	33.49	33.64
5	405	45	1350	13.5	211.5	56	400	50.05	48.24	50.04	50.03
6	405	45	1350	13.5	211.5	56	800	16.84	17.13	17.04	16.84

also be used to forecast future values that are unknown at the time. These results demonstrate that the data match the model well because of good training.

The neural network training error histograms for the back-propagation training algorithms for the compressive strength of WA-cement-NT-based mortar are also shown in Fig. 11. The histogram error indicated that around 9 occurrences of projected values for 7-4-1 network structure exhibited zero error at 0.0173%. Similarly, about 14 instances of 7–10-10-1 network architecture resulted in zero error between −0.023 and 0.024%. For 7-14-14-14-1 network structure, zero error between −0.1588 and 0.0779% for about 20 instances. Figs. 10 and 11 show that the data fit the model well as a result of good training and validation, which implies that a network system with superior training delivers results with the least amount of error and can also be used to predict the compressive strength of blended cement mortar modified with Nano TiO_2.

3.5.3. *Regression plots of training, testing, and validation*

The correlation coefficients for training, validation, testing, and the combined set for the compressive strength of mortar based on WA-cement-NT are shown in Fig. 12. As shown in Fig. 12, the total set of all the R-values for the Levenberg-Marquardt backpropagation training techniques of 7-4-1, 7-10-10-1, and 7-14-14-14-1 network structures were 99.843%, 99.99%, and 99.70%, respectively. The value of the regression coefficient denotes the correlation between the output and the desired (target) value. The output and the target have a perfect relationship when the R-value is 100%. Relevant studies have shown that a random relationship exists when R-value is zero and that results are of higher quality when R-value is greater than 90% [54,61–63]. As can be seen in Fig. 12, the regression plots exhibit a strong relationship.

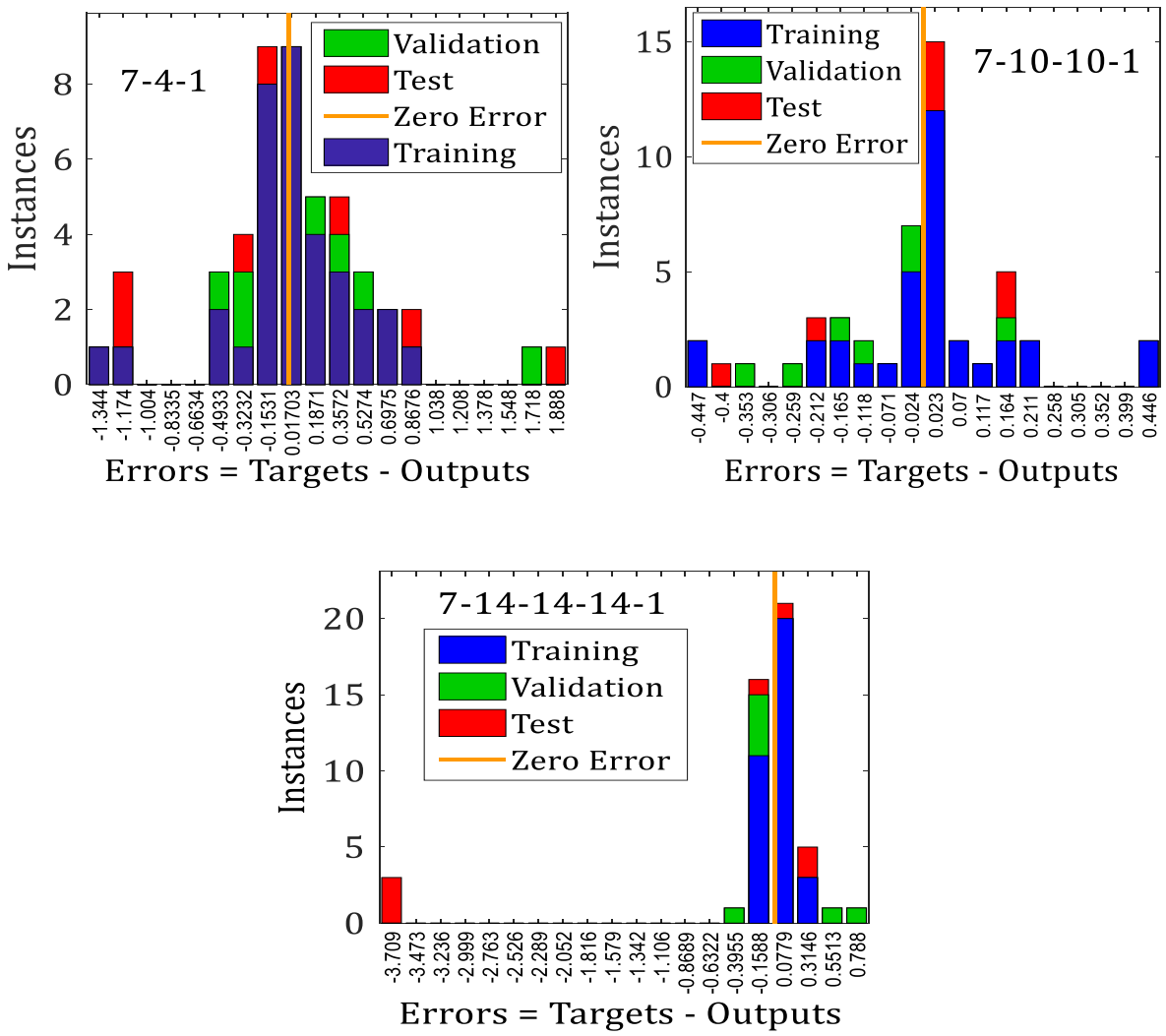

Fig. 11. Neural network training error histogram with 20 bins.

Aligning with a prior work, which used an ANN 5-11-1, the combined correlation coefficients of ANN predictions of cement mortar compressive strength were above 90% [57].

3.5.4. *Validation of developed network architectures with untrained datasets*

Making sure the model actually fulfils the required function involves validating it with data that were not observed during model training. Usually, this entails proving the model's accuracy in relation to the application for which it was intended. In particular, target data (compressive strength) and input data (cement, wood ash, silica sand, Nano titanium oxide, water, curing day, and temperature) were used to confirm the network structures that were built. The predicted responses for all trained network structures are presented in Table 9, while Table 10 shows the results of absolute and relative errors between the true and predicted responses. The errors arising from the analysis, as indicated in Table 10, are negligible. This indicates that the developed network architectures accurately predicted the compressive strength of WA-cement-NT-based mortar with a 95% confidence level and predictive ranges. The absolute errors of 0.37, 1.35, and 1.80 MPa indicated in Table 10 for 7-4-1, 7-10-10-1, and 7-14-14-14-1 network structures could be created by outliers.

The correlation between the true and predicted compressive strengths was analysed and the results are presented in Fig. 13. The model's accuracy increases and becomes stronger as R-value closes to 100%. However, a developed model is more accurate when the RMSE is farther from zero. According to Fig. 13, the coefficient of determination (R^2) and root mean square error (RMSE) values for validating the true and predicted responses were 99.65% and 0.8194 for 7-4-1 network architecture, 99.75% and 0.704 for 7-10-10-1 network structure, and 99.60% and 0.8923 for 7-14-14-14-1 network structure. These statistical findings indicated a strong correlation between the input and target arguments for the established network architectures.

4. Conclusions

This study investigated the effects of TiO_2 nanoparticles on wood ash-cement based mortar exposed to elevated temperatures. Levenberg–Marquardt backpropagation training techniques of different network structures developed from ANN was used to predict the compressive strength of mortar produced after high temperatures. The compressive strength results obtained in the ANN models were compared with the experimental results. Based on the experimental and computational findings, the following conclusions can be drawn:

i. As the temperature rises, mortar specimens lose weight more quickly. By incorporating 1% NT, weight loss was reduced to the barest minimum while the addition of WA increased the weight loss percentage.

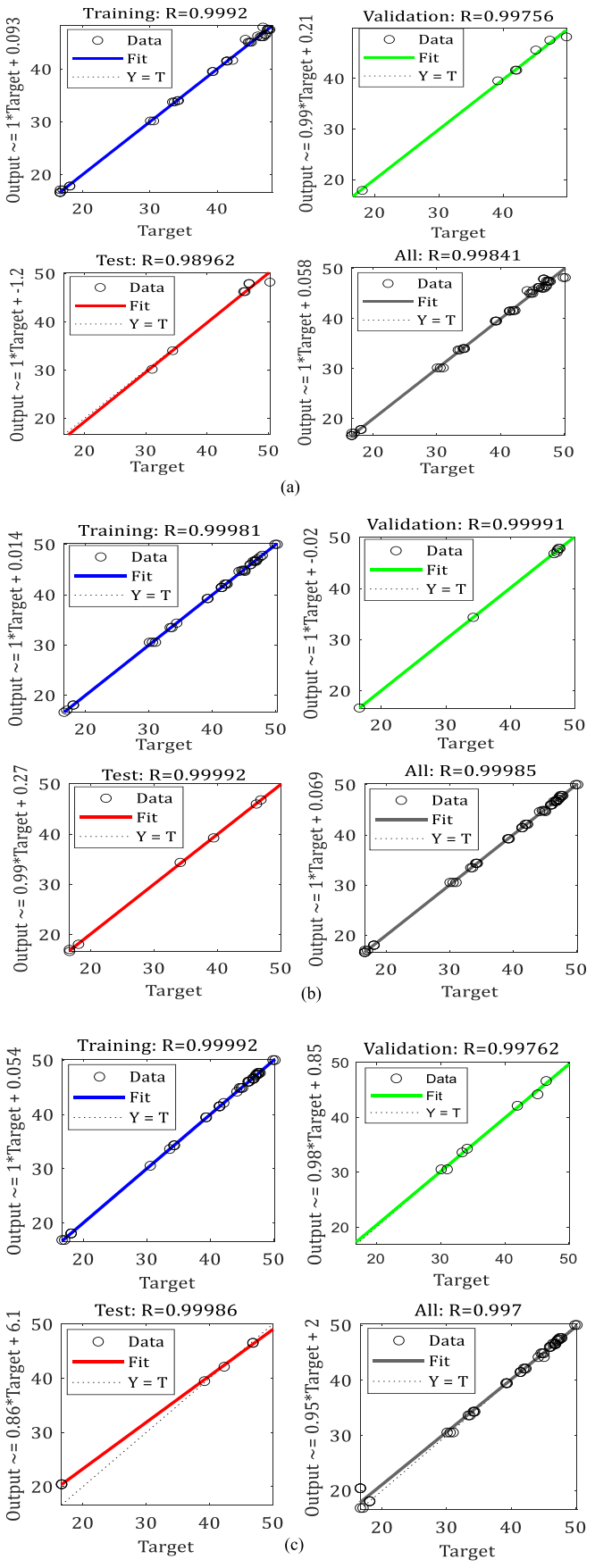

Fig. 12. Regression plots for (a) 7-4-1, (b) 7-10-10-1, and (c) 7-14-14-14-1 network architectures.

Table 10
Absolute and relative errors of the developed network structures.

S/N	Absolute error (MPa)			Relative error (%)		
	7-4-1	7-10-10-1	7-14-14-14-1	7-4-1	7-10-10-1	7-14-14-14-1
1	0.37	1.35	1.8	0.80	2.93	3.91
2	−0.53	−0.48	−0.36	−1.13	−1.02	−0.76
3	0.43	−0.15	−0.24	0.92	−0.32	−0.51
4	−0.27	0	−0.15	−0.81	0.00	−0.45
5	1.81	0.01	0.02	3.62	0.02	0.04
6	−0.29	−1.19	−0.02	−1.72	−1.19	−0.12

ii. The flexural strength of mortar specimens increased up to 200 °C and then dropped till an elevated temperature of 800 °C. The addition of WA and NT to the cement mortar did not significantly improve the flexural strength at high temperatures (400–800 °C).
iii. The compressive strength of all mortar specimens increased steadily up to burning at 400 °C and then decreased drastically between 400 and 800 °C of elevated temperatures. The addition of WA and NT slightly reduced the compressive strength. However, the addition of 3% NT marginally increased the compressive strength at 105–400 °C compared to 1 and 2% NT. Nevertheless, at 600–800 °C, addition of 2% NT to the mortar mix, to a slight extent, improved the compressive strength.
iv. Mortar specimens with 3% NT addition recorded the highest residual strength increases of between 18.75 and 27.38%. In addition, compared to compressive strength, flexural strength is more severely affected by high temperatures.
v. Comparing the number of hidden layers and neurons in the network architectures of Levenberg-Marquardt backpropagation training techniques, it was found that the network structure with the best performance for predicting compressive strength produced from WA-cement-NT based mortar was 7–10-10-1, which had two hidden layers and ten neurons in each layer.
vi. A 7-10-10-1 network architecture was 92.91 and 87.27% more error-free efficient than 7-4-1 and 7-14-14-14-1 network architectures in addition to having a strong correlation coefficient.
vii. The validation of developed network architectures with untrained datasets showed very good confidence in the prediction accuracy of the compressive strength of cement-based mortars.

The findings and modelling process of the present study can be used by researchers, designers and engineers interested in predicting the strength of cement-based mortars and in developing new eco-efficient compositions for a variety of applications in civil engineering. Finding the real number of hidden layers is still a very difficult task. Numerous scholars are still debating the precise and ideal number of hidden layers. Future research should be expanded to incorporate extensive training dataset application. The inability to identify the ideal structure using various studies is another drawback of the established models in this work. Therefore, it is advised to use some metaheuristic optimization techniques to improve the coefficients and weights of the created models. Additionally, a larger database of the mechanical properties of cement-based materials can be made available to create a novel ANN approach.

Authors' contribution statement

Prof. Akeem Raheem: Conceptualization, Data curation, Formal analysis, Funding acquisition, Investigation, Methodology, Resources, Writing – original draft. Prof. Bolanle Ikotun: Resources, Supervision, Validation, Writing – review & editing. Dr. Solomon Oyebisi: Funding acquisition, Software, Validation, Writing – review & editing. Prof. Anthony Ede: Funding acquisition, Writing – review & editing.

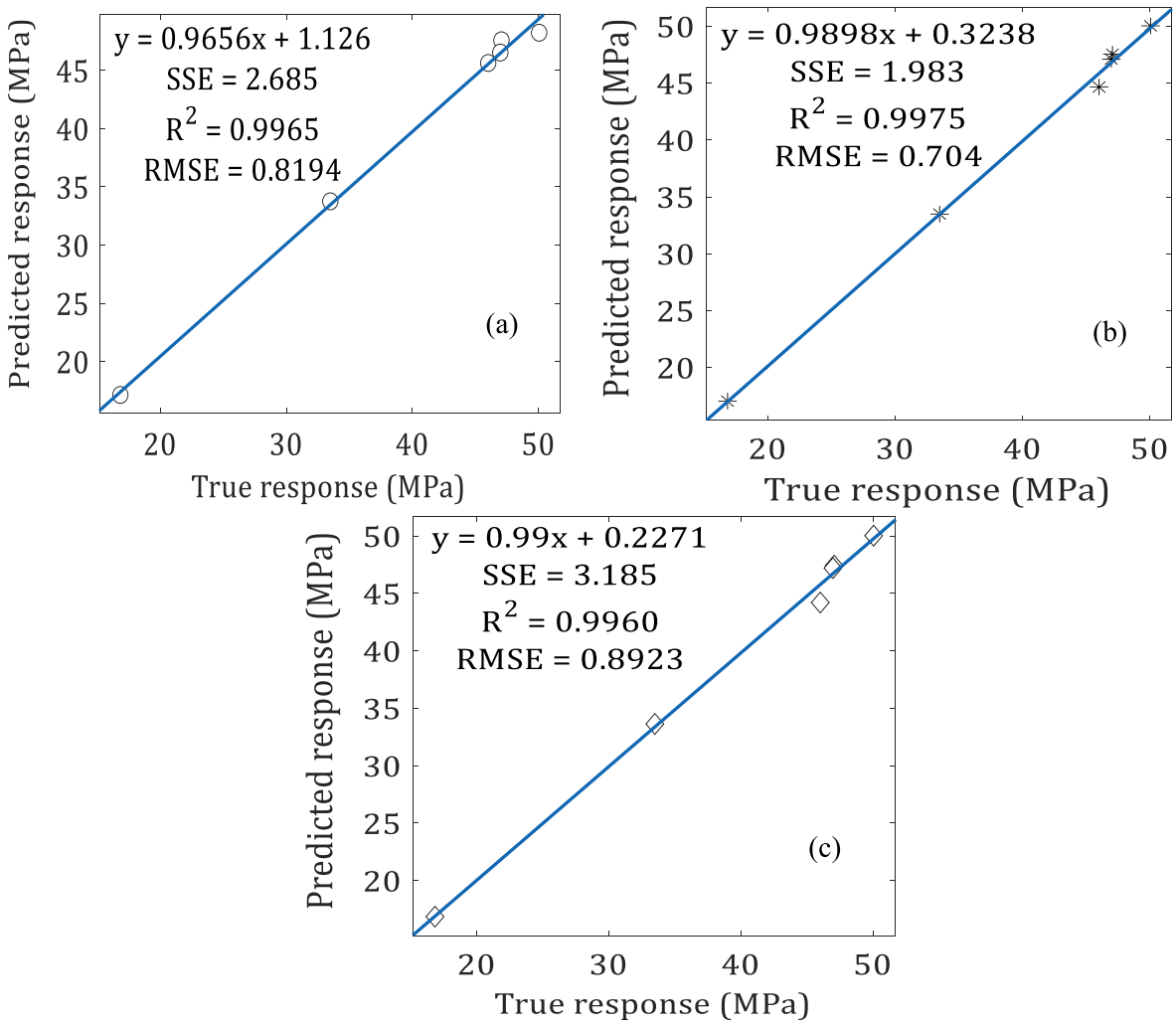

Fig. 13. Validation of developed ANNs with untrained samples for (a) 7-4-1, (b) 7-10-10-1, and (c) 7-14-14-14-1 network structures.

Funding

No support grant or financial aid was received by the authors for the conduct of this research.

Declaration of competing interest

The authors declare that they have no known competing financial interests or personal relationships that could have appeared to influence the work reported in this paper.

Data availability

All data used are included in the manuscript

Acknowledgments

The authors appreciated Prof. A. Lateef and Mr. P. O. Akinola for the process and synthesis of NT. The authors gratefully acknowledged the University of South Africa (UNISA) through the Research Support Program (VRSP) provided for first author, and thank Mr. Thulani and Sheila Mahlanga for providing the wood ash used in the study.

References

[1] S. Aydin, Development of a high temperature-resistant mortar by using slag and pumice, Fire Saf. J. 43 (2007) 610–617.
[2] O. Arioz, Effects of elevated temperatures on properties of concrete, Fire Saf. J. 42 (2007) 516–522.
[3] B. Demiral, O. Kelestemur, Effect of elevated temperature on the mechanical properties of concrete produced with finely ground pumice and silica fume, Fire Saf. J. 45 (2010) 385–391.
[4] M. Ismail, M.E. Ismail, B. Mohammed, Influence of elevated temperatures on physical and compressive strength properties of concrete containing palm oil fuel ash, Construct. Build. Mater. 25 (2011) 2358–2364.
[5] K.D. Hertz, Concrete strength for fire safety design, Mag. Concr. Res. 57 (8) (2005) 445–453.
[6] M. Kaya, M. Uysal, K. Yilmaz, C.D. Atis, Behaviour of geopolymer mortars after exposure to elevated temperatures, Mater. Sci. 24 (4) (2018) 428–438.
[7] H. Fanghui, W. Qiang, F. Jingjing, Differences among the role of ground fly ash in the paste, mortar and concrete, Construct. Build. Mater. 93 (2015) 172–179.
[8] A.A. Raheem, M.A. Kareem, Chemical composition and physical characteristics of rice husk ash blended cement, Int. J. Eng. Res. Afr. 32 (2017) 25–35.
[9] K. Ganesan, K. Rajagopal, K. Thangavel, Rice husk ash blended cement: assessment of optimal level of replacement for strength and permeability properties of concrete, Construct. Build. Mater. 22 (2008) 1675–1683.
[10] B. Chatveera, P. Lertwattanaruk, Evaluation of nitric and acetic acid resistance of cement mortars containing high-volume black rice husk ash, J. Environ. Manag. 133 (2014) 365–373.
[11] D.A. Adesanya, A.A. Raheem, Development of corn cob ash blended cement, Construct. Build. Mater. 23 (2009) 347–352.
[12] D.A. Adesanya, A.A. Raheem, A study of the permeability and acid attack of corn cob ash blended cements, Construct. Build. Mater. 24 (2010) 403–409.
[13] A.U. Elinwa, S.P. Ejeh, Effects of incorporation of saw dust incineration fly ash in cement pastes and mortar, J. Asian Architect. Build Eng. 3 (1) (2004) 1–7.
[14] A.A. Raheem, O.A. Adenuga, Wood ash from bread bakery as partial replacement for cement in concrete, Int. J. Sustain. Construct. Eng. Technol. 4 (1) (2013) 75–81.

[15] Z. Yang, J. Huddleston, H. Brown, Effects of wood ash on properties of concrete and flowable fill, J. Mater. Sci. Chem. Eng. 4 (2016) 101–114.
[16] M. Oltulu, R. Sahil, Single and combined effects of Nano-SiO_2, Nano-Al_2O_3 and Nano-Fe_2O_3 powders on compressive strength and capillary permeability of cement mortar containing silica fume, Mater. Sci. Eng. 528 (2011) 7012–7019.
[17] A. Benhood, H. Ziari, Effects of silica fume addition and water to cement ratio on the properties of high-strength concrete after exposure to high temperatures, Cement Concr. Compos. 30 (2008) 106–112.
[18] S. Oyebisi, T. Aloymari, Cement-based concrete modified with Vitellaria Paradoxa ash: a lifecycle assessment, Construct. Build. Mater. 342 (2022), 127906.
[19] S. Oyebisi, H. Owamah, T. Alomayri, A. Ede, Modeling the strength of cashew nutshell ash-cement-based concrete, Mag. Concr. Res. 74 (10) (2022) 487–496.
[20] A.M. Zeyad, M.A.M. Johari, M.A.M.B.A. Tayeh, M.O. Yusuf, Pozzolanic reactivity of ultrafine palm oil fuel ash waste on strength and durability performances of high strength concrete, J. Clean. Prod. 144 (2017) 511–522.
[21] A.S.M. Abdul Awal, I.A. Shehu, Performance evaluation of concrete containing high volume palm oil fuel ash exposed to elevated temperature, Construct. Build. Mater. 76 (2015) 214–220.
[22] S. Donatello, C. Kuenzel, A. Palomo, A. Fernandez-Jimenez, High temperature resistance of a high-volume fly ash cement paste, Cement Concr. Compos. 45 (2014) 234–242.
[23] S. Aydin, B. Baradan, Effect of pumice and fly ash incorporation on high temperature resistance of cement-based mortar, Cement Concr. Res. 37 (2007) 988–995.
[24] E. Horszczaruk, P. Sikora, K. Cendroswski, E. Mijowska, The effect of elevated temperature on the properties of cement mortars containing nanosilica and heavyweight aggregates, Construct. Build. Mater. 137 (2017) 420–431.
[25] R.K. Ibrahim, R. Hamid, M.R. Taha, Fire resistance of high-volume fly ash mortars with nanosilica addition, Construct. Build. Mater. 36 (2012) 779–786.
[26] F.C. Pereira, S.S. Borysov, Machine learning fundamentals (Chapter 2), in: C. Antoniou, L. Dimitriou, F. Pereira (Eds.), Pereira Big Data and Transport Analytics, Elsevier, Amsterdam, The Netherlands, 2019, pp. 9–29, 978-0-12-812970-8.
[27] P.G. Asteris, M. Koopialipoor, D.J. Armaghani, E.A. Kotsonis, P.B. Lourenço, Prediction of cement-based mortars compressive strength using machine learning techniques, Neural Comput. Appl. 33 (2021) 13089–13121.
[28] A.F. Bingol, A. Tortum, R. Gül, Neural networks analysis of compressive strength of lightweight concrete after high temperatures, Mater. Des. 52 (2013) 258–264.
[29] H.M. Najm, O. Nanayakkara, M. Ahmad, M.M. Sabri, Mechanical properties, crack width, and propagation of waste ceramic concrete subjected to elevated temperatures: a comprehensive study, Materials 15 (7) (2022) 2371.
[30] K.V.S. Ramana, T. Anita, S. Mandal, S. Kaliappan, H. Shaikh, P.V. Sivaprasad, et al., Effect of different environmental parameters on pitting behaviours of AISI type 316L stainless steel: experimental studies and neural network modelling, Mater. Des. 30 (2009) 3770–3775.
[31] A. Tortum, N. Yayla, M. Gökdag, The modelling of mode choices of intercity freight transportation with the artificial neural networks and adaptive neuro-fuzzy inference system, Expert Syst. Appl. 36 (3) (2009) 6199–6217.
[32] B.D. Ikotun, A.A. Raheem, Characteristics of wood ash cement mortar incorporating green-synthesized Nano-TiO_2, Int. J. Concrete Struct. Mater. 15 (19) (2021) 1–9.
[33] Pretoria Portland Cement (PPC), Product Data Sheet PPC Suretech 52.5 N Cement, 2018. www.ppc.co.za. (Accessed 19 September 2019). accessed.
[34] SANS 50197-1, Cement – Part 1: Composition, Specifications and Conformity Criteria for Common Cement, SABS, Pretoria, 2000.
[35] A. Lateef, M.A. Azeez, T.B. Asafa, T.A. Yekeen, A. Akinboro, I.C. Oladipo, L. Azeez, S.E. Ajibade, S.A. Ojo, E.B. Gueguim-Kana, L.S. Beukes, Biogenic synthesis of silver nanoparticles using pod extract of Cola nitida: antibacterial and antioxidant activities and application as a paint additive, J. Taibah Univ. Sci. 10 (2016) 551–562.
[36] A.A. Raheem, O.A. Adenuga, Wood ash from bread bakery as partial replacement for cement in concrete, Int. J. Sustain. Construct. Eng. Technol. 4 (1) (2013) 75–81.
[37] M. Berra, F. Carassiti, T. Mangialardi, A.E. Paolini, M. Sebastiani, Effects of nanosilica addition on workability and compressive strength of Portland cement pastes, Construct. Build. Mater. 35 (2012) 666–675.
[38] SANS 196-1, Method of Testing Cement – Determination of Strengths, SABS, Pretoria, 2006.
[39] A. Ababneh, M. Alhassan, M. Abu-Haifa, Predicting the contribution of recycled aggregate concrete to the shear capacity of beams without transverse reinforcement using artificial neural networks, Case Stud. Constr. Mater. 13 (2020), e00414.
[40] P. Kim, MATLAB Deep Learning with Machine Learning, Neural Networks and Artificial Intelligence, Softcover ISBN 978-1-4842-2844-9, Springer Book, Apress Berkeley, CA, 2017, https://doi.org/10.1007/978-1-4842-2845-6.
[41] M. Mohtasham Moein, A. Saradar, K. Rahmati, S.H. Ghasemzadeh Mousavinejad, J. Bristow, V. Aramali, M. Karakouzian, Predictive models for concrete properties using machine learning and deep learning approaches: a review, J. Build. Eng. 63 (2023), 105444.
[42] K. Hornik, Approximation capabilities of multilayer feedforward networks, Neural Network. 4 (2) (1991) 251–257.
[43] G.E. Hinton, S. Osindero, Y.W. Teh, A fast-learning algorithm for deep belief nets, Neural Comput. 18 (7) (2006) 1527–1554.
[44] J.I. Kim, D.K. Kim, M.Q. Feng, F. Yazdani, Application of neural networks for estimation of concrete strength, J. Mater. Civ. Eng. 16 (3) (2004) 257–264.
[45] M. Khandelwal, D.L. Kumar, M. Yellishetty, Application of soft computing to predict blast-induced ground vibration, Eng. Comput. 27 (2) (2011) 117–125.
[46] S. Rajasekaran, D. Suresh, G.V. Pai, Application of sequential learning neural networks to civil engineering modelling problems, Eng. Comput. 18 (2) (2002) 138–147.
[47] S. Tohidi, Y. Sharifi, Neural networks for inelastic distortional buckling capacity assessment of steel I-beams, Thin-Walled Struct. 94 (2015) 359–371.
[48] M. Mohammadhassani, H. Nezamabadi-Pour, M.Z. Jumaat, M. Jameel, A.M. S. Arumugam, Application of artificial neural networks (ANNs) and linear regressions (LR) to predict the deflection of concrete deep beams, Comput. Concr. 11 (3) (2013) 237–252.
[49] J. Schmidhuber, Deep learning in neural networks: an overview, Neural Network. 61 (2015) 85–117.
[50] L. Deng, Deep learning: methods and applications, Found. Trends Signal Process. 7 (2014) 197–387.
[51] H.-B. Ly, T.-A. Nguyen, H.-V. Thi Mai, V.Q. Tran, Development of deep neural network model to predict the compressive strength of rubber concrete, Construct. Build. Mater. 301 (2021), 124081.
[52] P.S.M. Thilakarathna, S. Seo, K.S.K. Baduge, H. Lee, P. Mendis, G. Foliente, Embodied carbon analysis and benchmarking emissions of high and ultra-high strength concrete using machine learning algorithms, J. Clean. Prod. 262 (2020), 121281.
[53] K.A. Patel, S. Chaudhary, A.K. Nagpal, An automated computationally efficient two-stage procedure for service load analysis of RC flexural members considering concrete cracking, Eng. Comput. 33 (3) (2017) 669–688.
[54] T. Gupta, K.A. Patel, S. Siddique, R.K. Sharma, S. Chaudhary, Prediction of mechanical properties of rubberised concrete exposed to elevated temperature using ANN, Measurement 147 (2019), 106870.
[55] K. Patel, S. Chaudhary, A. Nagpal, Neural network-based approach for rapid prediction of deflections in RC beams considering cracking, Comput. Concr. 19 (3) (2017) 293–303.
[56] S. Chithra, S.S. Kumar, K. Chinnaraju, F.A. Ashmita, A comparative study on the compressive strength prediction models for High Performance Concrete containing nano silica and copper slag using regression analysis and Artificial Neural Networks, Construct. Build. Mater. 114 (2016) 528–535.
[57] H. Eskandari-Naddaf, R. Kazemi, ANN prediction of cement mortar compressive strength, influence of cement strength class, Construct. Build. Mater. 138 (2017) 1–11.
[58] K. Patel, S. Chaudhary, A. Nagpal, Rapid prediction of inelastic bending moments in RC beams considering cracking, Comput. Concr. 18 (6) (2016) 1113–1134.
[59] P.G. Asteris, V.G. Mokos, Concrete compressive strength using artificial neural networks, Neural Comput. Appl. 32 (2020) 11807–11826.
[60] A. Saradar, P. Nemati, A.S. Paskiabi, M.M. Moein, H. Moez, E.H. Vishki, Prediction of mechanical properties of lightweight basalt fiber reinforced concrete containing silica fume and fly ash: experimental and numerical assessment, J. Build. Eng. 32 (2020), 101732.
[61] A.A. Shahmansouri, M. Yazdani, S. Ghanbari, H. Akbarzadeh Bengar, A. Jafari, H. Farrokh Ghatte, Artificial neural network model to predict the compressive strength of eco-friendly geopolymer concrete incorporating silica fume and natural zeolite, J. Clean. Prod. 279 (2021), 123697.
[62] D. Dao, H.-B. Ly, S. Trinh, T.-T. Le, B. Pham, Artificial intelligence approaches for prediction of compressive strength of geopolymer concrete, Materials 12 (2019) 983.
[63] U. Atici, Prediction of the strength of mineral admixture concrete using multivariable regression analysis and an artificial neural network, Expert Syst. Appl. 38 (2011) 9609–9618.
[64] Z.H. Duan, S.C. Kou, C.S. Poon, Using artificial neural networks for predicting the elastic modulus of recycled aggregate concrete, Construct. Build. Mater. 44 (2013) 524–532.
[65] J.C. Willmott, K. Matsuura, Advantages of the mean absolute error (MAE) over the root mean square error (RMSE) in assessing average model performance, Clim. Res. 30 (2005) 79–82.
[66] R.M. Martins, A.J.F. Bombard, Rheology of fresh cement paste with superplasticizer and nanosilica admixtures studied by response surface methodology, Mater. Struct. 45 (6) (2012) 905–921.
[67] R. Yu, P. Spesz, H.J.H. Brouwers, Effect of nano-silica on the hydration and microstructure development of Ultra-High-Performance Concrete (UHPC) with a low binder amount, Construct. Build. Mater. 65 (2014) 140–150.
[68] I. Janotka, T. Nurnbergerova, Effect of temperature on structural quality of the cement paste and high-strength concrete with silica fume, Nucl. Eng. Des. 235 (2005) 2019–2032.
[69] H. Fares, A. Noumowe, S. Remond, Self-consolidating concrete subjected to high temperature: mechanical and physicochemical properties, Cement Concr. Res. 39 (12) (2009) 1230–1238.
[70] M. Heikal, A. I Ali, M.N. Ismail, S. Awad, N.S. Ibrahim, Behaviour of composite cement pastes containing silica nano-particles at elevated temperature, Construct. Build. Mater. 70 (2014) 339–350.
[71] G. Wang, C. Zhang, B. Zhang, Q. Li, Z. Shui, Study on the high-temperature behaviour and rehydration characteristics of hardened cement paste, Fire Mater. 39 (2015) 741–750.
[72] M.S. Morsy, A.M. Rashad, H.A. El-Nouhy, Behavior of blended cement mortars containing nano-metakaolin at elevated temperatures, Construct. Build. Mater. 35 (2012) 900–905.
[73] M. Sivasakthi, R. Jeyalakshmi, N.P. Rajamane, Investigation of microstructure and thermomechanical properties of Nano-TiO_2 admixed geopolymer for thermal resistance applications, J. Mater. Eng. Perform. (2021), https://doi.org/10.1007/s11665-021-05708-1.

[74] C. Moro, V. Francioso, M. Velay-Lizancos, Nano-TiO_2 effects on high temperature resistance of recycled mortars, J. Clean. Prod. 263 (2020), 121581.
[75] M. Bastami, A. Chaboki-Khiabani, M. Baghbadrani, M. Kordi, Perfomance of high strength concretes at elevated temperatures, Scientia Iranica- Transactions A: Civ. Eng. 18 (2011) 1028–1036.
[76] W.W. Lin, T.D. Lin, L.J. Powers-Couche, Microstructure of fire-damaged concrete, ACI Mater. J. 93 (3) (1996) 199–205.
[77] C. Fan, F. Xiao, Y. Zhao, A short-term building cooling load prediction method using deep learning algorithms, Appl. Energy 195 (2017) 222–233.
[78] M.T. Hagan, M.B. Menhaj, Training feedforward networks with the Marquardt algorithm, IEEE Trans. Neural Network. 5 (1994) 989–993.
[79] N.M. Nawi, A. Khan, M.Z. Rehman, A new Levenberg marquardt based back propagation algorithm trained with cuckoo search, Proc. Technol. 11 (2013) 18–23.
[80] S. Karsoliya, Approximating number of hidden layer neurons in multiple hidden layer BPNN architecture, Int. J. Eng. Trends Technol. 3 (6) (2012) 714–717.
[81] T. Gupta, K. Raza, Optimizing deep neural network architecture: a Tabu search based approach, Neural Process. Lett. (2020), https://doi.org/10.1007/s11063-020-10234-7.
[82] G. Panchal, A. Ganatra, Y. Kosta, D. Panchal, Analysis of multilayer perceptron with multiple hidden neurons and hidden, Int. J. Comput Theory Eng. 3 (2) (2011) 332–337.
[83] M. Uzair, N. Jamil, Effects of Hidden Layers on the Efficiency of Neural Networks, IEEE 23rd International Multitopic Conference (INMIC), 2020, pp. 1–6.